03,01,05

Landau Levels of the Topological Semimetal CoSi near the Γ-Point and Their Contribution to the Orbital Magnetic Susceptibility

© D.A. Pshenay-Severin, S.A. Nikolaev, Y.V. Ivanov, A.T. Burkov

Ioffe Institute,
St. Petersburg, Russia

E-mail: d.pshenay@mail.ru

Received March 13, 2024
Revised March 28, 2024
Accepted April 12, 2024

The band structure of the topological semimetal CoSi in a magnetic field is studied. Using tight-binding model based on first-principle calculations, electronic spectrum was obtained over the entire Brillouin zone. Its features near the topological node at the Γ-point are studied in the $\mathbf{k} \cdot \mathbf{p}$ approximation using parameters obtained from *ab initio* calculations. Since the topological charge of the node is greater than unity, several chiral levels appear in the magnetic field, the number of which is consistent with the magnitude of the charge. The contribution of the spectrum region near the node at the Γ-point to the orbital magnetic susceptibility of CoSi is calculated and its differences from the case of an ordinary Weyl node are analyzed.

Keywords: band structure in a magnetic field, band structure topology, diamagnetism, paramagnetism, cobalt monosilicide.

DOI: 10.61011/PSS.2024.05.58494.53

1. Introduction

CoSi is a semimetal. It was studied as a promising thermoelectric material [1], but the topological properties of its band structure have been also of interest in recent years. CoSi crystallizes in the B20 cubic structure (space group $P2_13$, No. 198) that has no inversion center [2]. Features of the crystal structure lead to the fact that at the time-reversal invariant momentum points Γ and R of the Brillouin zone the emergence of multiply degenerate energy levels with a linear dispersion law in their vicinity is possible [3–6]. Therefore, CoSi appears to be a topological semimetal where, as opposed to the Dirac and Weyl semimetals, nodes at the Γ- and R-points have a topological charge equal to 4 in absolute value. Features of the band structure and presence of topological nodes have been proved by the angle-resolved photoelectron spectroscopy experiments [7–9].

Behavior of the Weyl semimetals in a magnetic field has a number of interesting features [10]. They include — chiral anomaly and negative magnetoresistance [11] that are associated with the Landau level spectrum in a magnetic field containing a zero chiral level where carriers can move only along or opposite to the field depending on the topological charge sign. These effects in CoSi were studied in [12]. In CoSi, quantum oscillations of resistance [13,14] and thermopower [15] were also examined in fields up to 15 T that were interpreted in view of features of the band structure and topological charges.

CoSi and isostructural materials demonstrate a wide variety of magnetic properties. CoSi single-crystals at temperatures above 25 K are diamagnetic materials, but at lower temperatures, magnetic susceptibility of most samples reverses the sign [16,17]. CoSi solid solutions with a low concentration of Fe are diamagnetic at room temperature, while ferromagnetic properties appear with an increase in Fe concentration [18]. In the isostructural material MnSi in low magnetic fields, a helical magnetic structure was revealed, which transforms into a ferromagnetic structure with increasing field [19,20]. A skyrmion phase may also appear in MnSi [21].

Magnetic susceptibility of topological semimetals also has some features. Susceptibility of the Weyl semimetals was investigated in several papers that are summarized in [22]. A giant diamagnetic anomaly characterized by divergence of susceptibility when chemical potential approaches the Weyl node energy was reported in [23]. This anomaly in the Weyl and Dirac semimetals was also studied in [24,25]. It was analyzed for an arbitrary tilt of the spectrum in [26]. The temperature dependence of susceptibility is also non-monotonic and has a minimum at $T \approx 0.443\,\mu/k_B$ [22], where μ is the chemical potential counted from the node energy, k_B is the Boltzmann constant. It is interesting that a similar feature was observed in the Weyl semimetal TaAs at approximately 185 K [27]. Examination of magnetization in TaAs in [28] has also shown that, as opposed to quasiparticles with a nonrelativistic spectrum, the Weyl semimetal has no saturation of longitudinal magnetization in strong fields.

For multi-Weyl semimetals, where a topological charge exceeding 1 is associated with non-linear dependence of energy on the wave vector in some directions, the spectrum in the magnetic field and the density of states were calculated in [29]. For fermions with preudospin 1 and liner dispersion law, the spectrum in the magnetic field was

reported in the Appendix to [3]. For fermions with higher pseudospins, the Landau levels were calculated in [30]. However, the magnetic susceptibility was not addressed in these papers.

In CoSi, low-energy excitations near Γ and R points without considering the spin-orbit interaction correspond to quasiparticles with pseudospin 1 (spin-1 fermions) [3,4] and double Weyl fermions [8], respectively. They feature a topological charge equal to 2 in absolute value. The spin-orbit interaction splits the multiplet at the Γ-point into the Weyl doublet and a fourfold degenerate level with a topological charge equal to 4 in absolute value. At the R-point, the multiplet is split into a doublet without a topological charge and a sixfold degenerate node with the same topological charge in absolute value, but of opposite sign. In addition, there are other topologically nontrivial points and band degeneracy planes in the Brillouin zone. Such a wide range of topological nodes found in CoSi gives a reason to the study of their splitting in a magnetic field and the resulting features of magnetic susceptibility.

2. Calculation of the electronic spectrum of CoSi in a magnetic field

The electronic spectrum was calculated using generalised gradient approximation for density functional in QuantumESPRESSO [31]. In our calculations we used norm-conserving relativistic pseudopotentials [32], kinetic energy cut-off of 80 Ry for expansion of wave functions in plane wave basis and a $8 \times 8 \times 8$ grid for integration over the Brillouin zone. The equilibrium lattice constant $a_0 = 4.438$ Å and atom positions were taken from [33]. The calculation was performed both without and with the account of spin-orbit interaction (SOC), and the corresponding band structures are shown in Figure 1 in [33].

The calculated Bloch functions and energies on the above-mentioned grid were used to construct the tight-binding Hamiltonian in Wannier90 [34]. Then, the electronic spectrum in the magnetic field was calculated using WannierTools package [35]. The magnetic field influence was considered in the tight-binding Hamiltonian through the Peierls substitution [36]. The magnetic field was oriented along the z axis, and a magnetic supercell consisting of q unit cells of crystal was formed in a plane perpendicular to the field. The magnetic B-field strength was defined in such a way that an integer number of p quanta of flux $\Phi_0 = 2\pi\hbar c/e$, i.e. $B = p\Phi_0/(qa_0^2)$, flows through the magnetic supercell area. The experimentally available magnetic fields are about 15 T [12–15] that corresponds to the magnetic supercell size $q = 1400$. A larger cell size requires considerable computational resources and limits from below the magnetic field range available for calculation in the tight-binding model. In low magnetic fields, the electronic spectrum near Γ-point may be calculated using $\mathbf{k}\cdot\mathbf{p}$ approximation.

Without considering the spin-orbit interaction and magnetic field, the Hamiltonian at the Γ-point corresponds to quasiparticles with pseudospin 1, it was used in [33] to study the influence of deformation on the topological properties of CoSi. The Hamiltonian can be calculated as follows.

Decomposition of the group of the wave vector at the Γ-point of the Brillouin zone with respect to the translation subgroup leads to a factor group isomorphic to the point group $T(23)$. It has 3 one-dimensional representations Γ_1, Γ_2, Γ_3 and one three-dimensional representation Γ_4, according to which both a vector and a pseudovector are transformed due to the absence of the inversion center. We are interested in a threefold degenerate level at the Γ-point. The electron wave functions of this level $|X\rangle$, $|Y\rangle$ and $|Z\rangle$ are transformed according to the representation Γ_4 as radius vector projections. CoSi is a cubic crystal, but its symmetry group does not contain an inversion, therefore matrix elements of the momentum operator on the chosen basis functions may be non-zero. To see this it is sufficient to show that the direct product of representations according to which the wave functions and their complex conjugates transform contains the representation according to which momentum components transform. As a matter of fact, $\Gamma_4 \otimes \Gamma_4^* = \Gamma_1 \oplus \Gamma_2 \oplus \Gamma_3 \oplus 2\Gamma_4$ contains Γ_4, therefore some momentum matrix elements should be non-zero. The analysis shows that, taking into account the time reversal symmetry, the matrix elements $\langle X|\hat{p}_y|Z\rangle = \langle Y|\hat{p}_z|X\rangle = \langle Z|\hat{p}_x|Y\rangle$ are non-zero, therefore the Hamiltonian expansion in powers of the wave vector starts with linear terms. According to the method of invariants, the $\mathbf{k}\cdot\mathbf{p}$-Hamiltonian may be written as $\hat{H}^{(1)} = \Sigma_\nu a_\nu \Sigma_i X_i^\nu K_i^{\nu *}$, where $K_i^{\nu *}$ is the combinations of wave vector components transforming according to the representation ν, X_i^ν is the basis matrices transforming according to the same representation and a_ν are constants. Since only terms linear in $\mathbf{k}$ are included in the Hamiltonian, wave vector components transforming according to the representation Γ_4 should be used instead of $K_i^{\nu *}$. The basis matrices X_i^ν may be chosen in the form of linear combinations of nine independent matrices $\hat{1}$, $\hat{J}_x$, $\hat{J}_y$, $\hat{J}_z$, $\hat{J}_x^2$, $\hat{J}_y^2$, $\{\hat{J}_x, \hat{J}_y\}$, $\{\hat{J}_y, \hat{J}_z\}$, $\{\hat{J}_z, \hat{J}_x\}$, where $\hat{J}_{x(y,z)}$ are the matrices of the projections of the angular momentum 1 [37]. Among them, two sets $\hat{J}_x$, $\hat{J}_y$, $\hat{J}_z$ and $\{\hat{J}_y, \hat{J}_z\}$, $\{\hat{J}_z, \hat{J}_x\}$, $\{\hat{J}_x, \hat{J}_y\}$ transform according to the representation Γ_4 as are the wave vector components k_x, k_y, k_z. Taking into account the symmetry with respect to time reversal, the first of them must be chosen, and the Hamiltonian may be written as $\hat{H}^{(1)} = \hbar v \hat{\mathbf{J}}\cdot\hat{\mathbf{k}}$, where v is the electron velocity. In our case, it is more convenient to switch to a canonical basis $|Y_1^1\rangle = (-i|X\rangle + |Y\rangle)/\sqrt{2}$, $|Y_0^1\rangle = i|Z\rangle$, $|Y_{-1}^1\rangle = (i|X\rangle + |Y\rangle)/\sqrt{2}$ [38] where the Hamiltonian will be equal to

$$\hat{H}^{(1)} = \hbar v \begin{pmatrix} k_z & \frac{k_x - ik_y}{\sqrt{2}} & 0 \\ \frac{k_x + ik_y}{\sqrt{2}} & 0 & \frac{k_x - ik_y}{\sqrt{2}} \\ 0 & \frac{k_x + ik_y}{\sqrt{2}} & -k_z \end{pmatrix}. \quad (1)$$

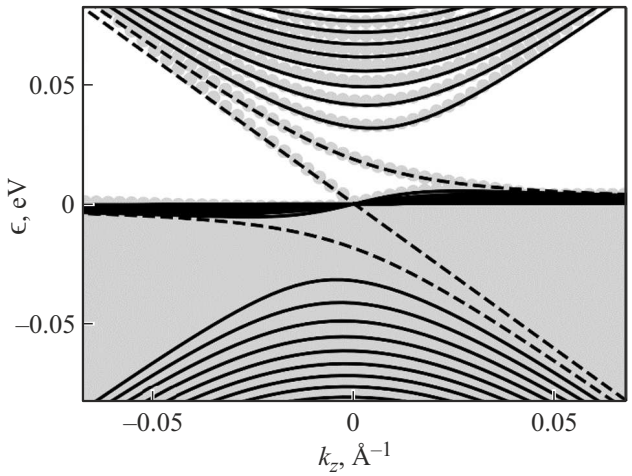

Figure 1. The electronic spectrum of CoSi in a 15 T magnetic field without considering spin-orbit interaction. Symbols — the tight-binding model calculation, lines — the $\mathbf{k}\cdot\mathbf{p}$ calculation (chiral levels are shown as dashed lines and three series of levels with $n \geq 0$ are shown as solid lines).

The influence of the magnetic field is taken into account by replacing the momentum $\hbar\mathbf{k}$ with operator $\hat{\pi} = \hbar\hat{\mathbf{k}} + e\mathbf{A}/c$. In the Landau gauge, the vector potential $\mathbf{A} = (0, Bx, 0)$. Let us introduce the raising and lowering operators using the relations

$$\hat{a}^+ = (\hat{\pi}_x + i\hat{\pi}_y)/(i\sqrt{2b}\hbar), \quad \hat{a} = -(\hat{\pi}_x - i\hat{\pi}_y)/(i\sqrt{2b}\hbar),$$

where b is proportional to the magnetic field: $b = eB/(\hbar c)$ and is related to the magnetic length by the relation $b = l^{-2}$. As a result, the Hamiltonian is written as

$$\hat{H}_B^{(1)} = \hbar v \begin{pmatrix} k_z & -i\sqrt{b}\hat{a} & 0 \\ i\sqrt{b}\hat{a}^+ & 0 & -i\sqrt{b}\hat{a} \\ 0 & i\sqrt{b}\hat{a}^+ & -k_z \end{pmatrix}, \qquad (2)$$

where k_z is the projection of the wave vector in the field direction.

The eigenvector components can be sought for in the form of expansion in wave functions of the harmonic oscillator $\phi_n(x)$: $\psi_i(x) = \Sigma_n c_i^{(n)}\phi_n(x)$, $i = 1, 2, 3$, where n is the oscillator level number [39]. Substitution of $\psi_i(x)$ in the Schrödinger equation with the Hamiltonian (2) results in a system of equations with an infinite number of variables $c_i^{(n)}$. Fortunately, this system can be divided into systems of linear equations in three unknown variables $c_1^{(n)}$, $c_2^{(n+1)}$, $c_3^{(n+2)}$, if we take into account the orthogonality of the functions $\phi_n(x)$ and replace n by $n+1$ $(n+2)$ in expansions of ψ_2 (ψ_3). For the given n, such system of equations will be written as $\hat{H}\mathbf{c} = \epsilon\mathbf{c}$, where $\mathbf{c} = (c_1^{(n)}, c_2^{(n+1)}, c_3^{(n+2)})^{\mathrm{T}}$,

$$\hat{H} = \hbar v \begin{pmatrix} k_z & -i\sqrt{b(n+1)} & 0 \\ i\sqrt{b(n+1)} & 0 & -i\sqrt{b(n+2)} \\ 0 & i\sqrt{b(n+2)} & -k_z \end{pmatrix}. \qquad (3)$$

The solutions of the secular equation of this system determine the Landau levels. Since $c_i^{(n)} = 0$ at $n < 0$, this system must be solved for integer $n \geq -2$. The energy levels for $n \geq 0$ are determined from the cubic equation

$$\epsilon^3 - (\hbar v)^2(k_z^2 + (2n+3)b)\epsilon + (\hbar v)^3 b k_z = 0. \qquad (4)$$

For each n, three solutions are achieved and form three Landau level subbands (see Figure 1). The corresponding stationary state vectors have three non-zero components.

At $n = -2$ (-1), the first and second (first) elements of column $\mathbf{c}$ should be zeroed. The spectrum is achieved by solving the secular equation obtained by removing the first and second (first) columns and rows from the matrix (3). Energies of these chiral Landau levels are equal to $\epsilon_\chi^{(1)} = -\hbar v k_z$, $\epsilon_\chi^{(2,3)} = \hbar v(-k_z \pm \sqrt{k_z^2 + 4b})/2$. The corresponding stationary state vectors are equal to $\psi_\chi^{(1)} = (0, 0, \phi_0)$ and $\psi_\chi^{(2,3)} = (0, i\sqrt{b}\phi_0, -(\epsilon/\hbar v)\phi_1)/\sqrt{(\epsilon/\hbar v)^2 + b}$.

The electronic spectrum of CoSi in the magnetic field obtained without considering the spin-orbit interaction is shown in Figure 1, where $\hbar v = 1.22\,\text{eV Å}$ was used [33]. This agrees with those obtained in [3,30]. In [3], it was discussed in connection with the description of low-energy excitations near P-point of the Brillouin zone of a cubic body-centered lattice belonging to space group No. 199, where $\mathbf{k}\cdot\mathbf{p}$-Hamiltonian also corresponded to quasiparticles with spin 1. In [30], in addition to quasiparticles with pseudospin 1, the Landau levels for quasiparticles with pseudospins 3/2 and 2 were also addressed.

For the Weyl node with topological charge 1, there is one chiral level and two series of the Landau levels that form the conduction band and valence band states. In our case, the topological charge of the node is equal to 2. In accordance with this, there shall be two chiral levels (shown dashed in Figure 1). One of them $\epsilon_\chi^{(1)}$ is shown as a single line and coincides with that for an ordinary Weyl node at the same v. The second chiral level consists of two parts $\epsilon_\chi^{(2,3)}$.

States for $n \geq 0$ form three bands: a valence band, a conduction band and a narrow band in the center. The states in the valence band and conduction band, as opposed to the Weyl node, are not symmetrical with respect to $k_z = 0$, but the electronic spectrum in general is the odd function of k_z. Extremum positions in the conduction band and valence band

$$\epsilon_{c(v)} = \pm\hbar v\sqrt{(3 + 2\sqrt{2})b/2}$$

correspond to points

$$k_z = \pm\sqrt{b/(6 + 4\sqrt{2})}.$$

These spectrum branches in this approximation are not limited from above and below, however, a natural limitation is the region of wave vectors $|k_z| \leq k_0$ and energies $|\epsilon| \leq \epsilon_0 = \hbar v k_0$, where $\mathbf{k}\cdot\mathbf{p}$ method matches well with the band structure of this material. For estimations in CoSi, $k_0 = 0.071\,\text{Å}^{-1}$ and $\epsilon_0 = 0.087\,\text{eV}$ were used.

A feature of the spectrum of quasiparticles with pseudospin 1 in the magnetic field is the presence of the energy-limited narrow band with high density of states. The energy limits are equal to $\pm\epsilon_m$, where $\epsilon_m = \hbar v\sqrt{(3-2\sqrt{2})b/2}$, and are achieved at $k_z = \pm\sqrt{b/(6-4\sqrt{2})}$.

Figure 1 shows that the $\mathbf{k}\cdot\mathbf{p}$ method and the tight-binding method match well at energies higher than the energy of Γ node without field ϵ_Γ. At $\epsilon < \epsilon_\Gamma$, points in the tight-binding method merge with each other (the gray region in Figure 1). Differences at $\epsilon < \epsilon_\Gamma$ are associated with the fact that the tight-binding method includes the contribution of other states, for example, of peak in M-point, that overlap with the spectrum in the valence band near Γ-point (see Figure 1 in [33]).

To consider the spin-orbit interaction, the basis of electronic states was expanded to take into account the spin component $|Y_m^1\rangle \otimes |\uparrow\rangle$, $|Y_m^1\rangle \otimes |\downarrow\rangle$, $m = 1,\ 0,\ -1$. In this basis, the spin-orbit interaction operator in the zeroth order approximation in the wave vector is written as

$$\hat{H}^{SOC} = \begin{pmatrix} \Delta & 0 & 0 & 0 & 0 & 0 \\ 0 & -\Delta & \sqrt{2}\Delta & 0 & 0 & 0 \\ 0 & \sqrt{2}\Delta & 0 & 0 & 0 & 0 \\ 0 & 0 & 0 & 0 & \sqrt{2}\Delta & 0 \\ 0 & 0 & 0 & \sqrt{2}\Delta & -\Delta & 0 \\ 0 & 0 & 0 & 0 & 0 & \Delta \end{pmatrix}. \quad (5)$$

In view of SOC, the 6-fold degenerate level at the Γ-point is split into 4- and 2-fold degenerate levels with energy shift by Δ and -2Δ, respectively (Figure 2). Near Γ-point, the Hamiltonian is written as $\hat{H} = \hat{H}^{(1)} \otimes \hat{1}_{2\times 2} + \hat{H}^{SOC}$. The spin-orbit splitting magnitude was obtained from *ab initio* calculations and was equal to $\Delta = 18$ MeV.

The spectrum in the magnetic field may be calculated in a similar way by introducing the vector potential into the momentum operator and proceeding to the raising and lowering operators. The Zeeman splitting may be considered using an additional term $\hat{H}^{(Z)} = \mu_B B \hat{1}_{3\times 3} \otimes \hat{\sigma}_3$, where μ_B is the Bohr magneton, $\hat{\sigma}_3$ is the Pauli matrix. The column of coefficients of state vector expansion over oscillatory functions in this case contains six components $\mathbf{c} = (c_1^{(n)}, c_2^{(n+1)}, c_3^{(n+1)}, c_4^{(n+2)}, c_5^{(n+2)}, c_6^{(n+3)})^{\mathrm{T}}$, and matrix $\hat{H}$ is written as

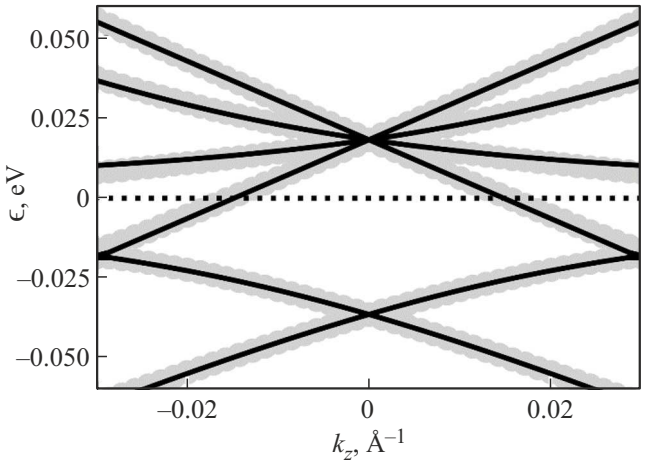

Figure 2. The electronic spectrum of CoSi near Γ-point with the account of the spin-orbit interaction obtained using $\mathbf{k}\cdot\mathbf{p}$ approximation (lines) and *ab initio* calculation (dots).

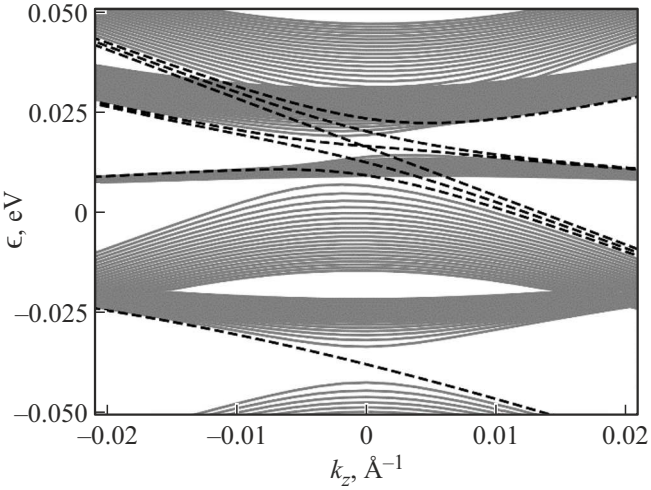

Figure 3. The electronic spectrum of CoSi near Γ-point in a 1 T magnetic field with spin-orbit interaction. The first 20 Landau levels are shown for each subband.

The spectrum in the 1 T magnetic field is shown in Figure 3. At such relatively low fields, spin-orbit splitting appears to be higher than level splitting in the magnetic field, and the Landau level related to quasiparticles with pseudospin 3/2 (four upper bands, $j = 3/2$) and the Weyl

$$\hat{H} = \hbar v \begin{pmatrix} \Delta^* + k_z + \mu^* b & 0 & -i\sqrt{b(n+1)} & 0 & 0 & 0 \\ 0 & -\Delta^* + k_z - \mu^* b & \sqrt{2}\Delta^* & -i\sqrt{b(n+2)} & 0 & 0 \\ i\sqrt{b(n+1)} & \sqrt{2}\Delta^* & \mu^* b & 0 & -i\sqrt{b(n+2)} & 0 \\ 0 & i\sqrt{b(n+2)} & 0 & -\mu^* b & \sqrt{2}\Delta^* & -i\sqrt{b(n+3)} \\ 0 & 0 & i\sqrt{b(n+2)} & \sqrt{2}\Delta^* & -\Delta^* - k_z + \mu^* b & 0 \\ 0 & 0 & 0 & i\sqrt{b(n+3)} & 0 & \Delta^* - k_z - \mu^* b \end{pmatrix}, \quad (6)$$

where $\Delta^* = \Delta/(\hbar v)$, $\mu^* = \mu_B c/(ev)$.

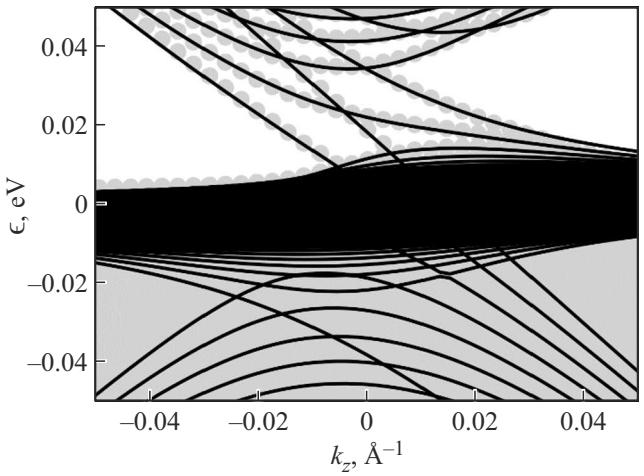

Figure 4. The electronic spectrum of CoSi near Γ-point in a 15 T magnetic field with spin-orbit interaction. Symbols — tight-binding model calculation, lines — calculation in $\mathbf{k}\cdot\mathbf{p}$ approximation.

fermions (two lower bands, $j = 1/2$) can be seen in the energy band diagram. They are derived from the secular equation at $n \geq 0$. At $n = -1$, -2 and -3, the system order decreases and 9 additional levels occur. Two of them appear to be the ordinary levels and are related to the Weyl fermion levels with the lowest numbers. Other seven levels are shown dashed in Figure 3. Six of them couple 4 upper bands and one of them couples 2 lower bands. Only 5 of these levels appear to be chiral: 4 for quasiparticles with preudospin 3/2 and 1 for the Weyl fermions, which agrees with the topologocal charges equal to 4 and 1, respectively. Such band pattern approximately corresponds to the spectra of quasiparticles with pseudospin 3/2 and the Weyl fermion spectra in the magnetic field that were calculated before, for example, in [30]. Distortions compared with [30] are caused in CoSi by interaction of the abovementioned bands. This interaction results, in particular, to the facts that the energies of states $j = 3/2$, $m = -1/2$ and $j = 1/2$, $m = 1/2$ weakly depend on the number of the Landau level n resulting in appearance of region of high density of states in the center of the spectrum.

In the 15 T field, subband shifts in the magnetic field are comparable with the magnitude of spin-orbit splitting Δ (see Figure 4). The Landau levels originating from the states of quasiparticles with pseudospin 3/2 and the Weyl fermions are strongly overlapping: states with $j = 1/2$, $m = 1/2$ move up and form, together with $j = 3/2$, $m = -1/2$, a region of high density of states near the chemical potential. This region is similar to that obtained without considering SOC (Figure 1). Above it, 4 chiral levels and states of bands $j = 3/2$, $m = 1/2$ (3/2) are located. Figure 4 shows that, as without SOC, the $\mathbf{k}\cdot\mathbf{p}$ method and the tight-binding method match well at the energies higher than the energies of the Γ node without field ϵ_Γ and differences at $\epsilon < \epsilon_\Gamma$ are associated with the contributions of states from other regions of the Brillouin zone.

3. Orbital magnetic susceptibility of quasiparticles with pseudospin 1

The magnitude of magnetic susceptibility in material is defined by all filled states, however, its variation depending on the temperature and chemical potential μ is defined by the spectrum region near μ. The effect of topological nodes on the susceptibility variation will be manifested, if the chemical potential is near the node energy. According to [22,24,25], the contributions to the magnetic susceptibility may be divided into those from the spectrum region near the node limited by the energy range $\pm\epsilon_0$ and those from other parts of spectrum giving the background contribution. In [22,24,25], contribution to the susceptibility from the first and second types of Weyl nodes was studied. In CoSi, the chemical potential is near the node energy at the Γ-point. As shown above, the Landau level spectrum in CoSi appears to be quite complicated, in particular, considering SOC. However, both with and without considering SOC, the chemical potential is in the region of high density of states, and this is the difference of this spectrum from the Weyl fermion spectrum. The simplest description of this feature is provided when the spectrum of quasiparticles with pseudospin 1 in the magnetic field is examined when the peak of the density of states is associated with the Landau levels of the middle dispersionless band. Therefore, the study addresses the orbital contribution to the susceptibility of quasiparticles with pseudospin 1 without considering the spin-orbit interaction and Zeeman splitting in the limit of weak magnetic fields for which it was possible to derive an analytical expression.

To calculate the susceptibility, it is necessary to calculate the thermodynamic potential of a unit volume of substance depending on the magnetic field

$$\Omega_i = -\frac{bk_BT}{2\pi^2} \times \int_{-k_0}^{k_0} dk_z \sum_n \ln\left(1 + \exp\left(\frac{\mu - \epsilon_i(n, k_z, b)}{k_BT}\right)\right), \quad (7)$$

where i indicates the contributions of the states of conduction band (Ω_c), valence band (Ω_v), chiral levels (Ω_χ) and a narrow band in the center (Ω_m). In (7), μ is the chemical potential that is counted from the node energy at the Γ-point, $k_0 = \epsilon_0/\hbar v$, and the energy $\epsilon(n, k_z, b)$ is the function of the Landau level number n, wave vector along field k_z and magnetic field $B \propto b$. Expression (7) takes into account twofold spin degeneracy. Then, the magnetic susceptibility is defined as $\chi = -\partial^2\Omega/\partial B^2 = -(e/\hbar c)^2\partial^2\Omega/\partial b^2$. In the given case of low magnetic fields, contribution to the diamagnetic susceptibility from the Landau levels in the conduction band and valence band may be found by passing from summation over n to integration over energy using the Euler-Maclaurin equation. Integration is performed from $-\epsilon_0$ to ϵ_0, and the required derivatives from energy may be taken using the secular equation.

For the Weyl semimetal, the chiral level does not depend on the magnetic field and does not contribute to the susceptibility. For quasiparticles with pseudospin 1, the second chiral level consisting of two parts depends on the magnetic field. The total contribution to the diamagnetic susceptibility from the valence band, conduction band and parts of the second chiral level adjacent to these bands, χ_{cv}, appears to coincide with the contribution to the diamagnetic susceptibility of the Weyl node reported in [22]:

$$\chi_{cv} = -\frac{v}{6\pi^2\hbar}\left(\frac{e}{c}\right)^2 \int_0^{\epsilon_0} \frac{d\epsilon}{\epsilon}\Big(f_0(-\epsilon) - f_0(\epsilon)\Big), \qquad (8)$$

where $f_0(\epsilon) = 1/(1+\exp[(\epsilon-\mu)/(k_BT)])$ is the Fermi distribution function. As shown in [22], dependence of susceptibility on the chemical potential $\chi_{cv} \approx -ve^2/(6\pi^2c^2\hbar)\ln(\epsilon_0/|\mu|)$ at low temperatures logarithmically diverges at $\mu = 0$.

For quasiparticles with pseudospin 1, contribution of the narrow middle band shall be also considered. The feature of its spectrum is in that it occupies a finite energy range. As opposed to other bands, all Landau levels of the narrow band in the magnetic field are within this finite range $\pm\epsilon_m$. This results in occurrence of the peak of density of states near the node energy and the magnetic susceptibility in a weak field appears to be equal to

$$\chi_m = \frac{v^2k_0}{2\pi^2}\frac{\mathrm{arctg}(\sqrt{3/2})}{\sqrt{3/2}}\left(\frac{e}{c}\right)^2\left(-\frac{\partial f_0}{\partial\epsilon}\right)_{\epsilon=0}. \qquad (9)$$

Contribution of χ_{cv} to the orbital susceptibility appears to be negative and corresponding to a conventional diamagnetic contribution and contribution of χ_m appears to be positive. Dependences of both contributions on the chemical potential have a sharp peak near the node energy, but different magnitude and functional form.

Figure 5 shows dependences of the contribution of topological nodes to the orbital susceptibility on the chemical potential at 50 K. The susceptibility of the Weyl semimetal is negative and grows in absolute value when μ approaches the node energy. The orbital susceptibility of quasiparticles with pseudospin 1 coincides with the Weyl susceptibility when μ moves away from the node energy. When μ approaches the node energy, contribution of χ_m to the orbital susceptibility appears to be prevailing and the susceptibility changes sign.

Ab initio calculations show that in stoichiometric CoSi at low temperatures the chemical potential is located lower than the energy of node at the Γ-point approximately by 0.01 eV. The chemical potential depends on the temperature and may be changed intentionally by means of doping. When the temperature rises to room temperature, the chemical potential increases by approximately 0.02 eV, i. e. changes within ±0.01 eV near the node. For comparison with the Weyl semimetal, Figure 6 shows the temperature dependences of susceptibility for fixed chemical potentials from the abovementioned range: $\mu = -0.003$ and 0.01 eV. While the susceptibility for the Weyl node is negative

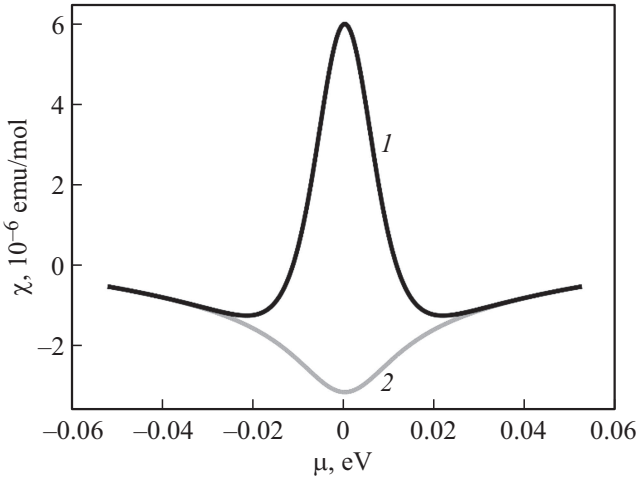

Figure 5. Dependence of the orbital susceptibility on the chemical potential for quasiparticles with pseudospin 1 (curve *1*) and for the Weyl node (2) at 50 K.

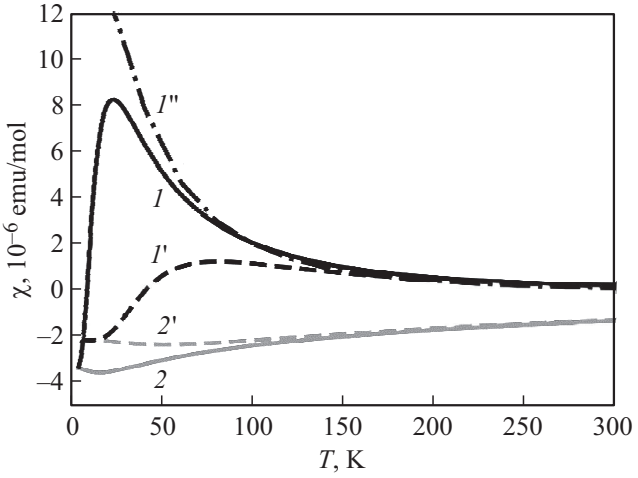

Figure 6. Dependence of the orbital susceptibility on temperature for quasiparticles with pseudospin 1 (curves *1, 1′, 1″*) and for the Weyl node (*2, 2′*) at $\mu = -0.003$ eV (*1, 2*) and 0.01 eV (*1′, 2′*), and also considering $\mu(T)$ (*1″*) (see the explanations in the text).

and has minimum in the temperature dependence, it is positive for the quasiparticles with pseudospin 1 and its temperature dependence has a peak. Extrema on the temperature dependences in both cases are more distinctive when the chemical potential approaches the node energy. The chemical potential position in CoSi changes when cobalt is substituted by other 3d metals. For example, when Co is substituted by Fe, the chemical potential moves down, and when Co is substituted by Ni — the chemical potential moves up along the energy. Curve *1″* in Figure 6 was plotted considering the dependence of the chemical potential on the temperature at constant concentration of carriers corresponding to 0.6 at.% of Ni. In this case, the chemical potential at 50 K coincides with the node energy resulting in dramatic growth of susceptibility.

A non-monotonic dependence of susceptibility on temperature was observed, for example, in the Weyl semimetal TaAs whose temperature dependence of susceptibility had a minimum at about 185 K [27]. Higher diamagnetic susceptibilities in graphene were discussed in [40] that reported their relation to the contribution of virtual interband transitions. Change of sign of the orbital susceptibility in a graphene type two-dimensional lattice was addressed in [41]. It was shown therein that the orbital susceptibility changes sign from diamagnetic to paramagnetic in transition from graphene to the dice lattice that is formed when an atom is added to the center of graphene hexagons. As shown in [42] when two-dimensional lattices were discussed, the orbital susceptibility always appears to be paramagnetic (positive) when the chemical potential is near the saddle point of the band structure.

The magnetic susceptibility in CoSi was experimentally studied in [16], which showed that it is of a diamagnetic nature (negative) at high temperatures. When the temperature decreased in the most pure samples, the susceptibility increased and changed sign to positive at a temperature below 25 K achieving 10^{-5} emu/mole. In [16] it was supposed that this might be due to the manifestation of antiferromagnetic interaction at low temperatures. Estimations shown in Figure 6 demonstrate similar temperature dependence and order of magnitude that gives ground to suggest that the contribution of topological states to the magnetic susceptibility of CoSi is exhibited. This feature of susceptibility of CoSi requires additional investigation taking into account the contribution to susceptibility not only of topological states near Γ-point, but also of other spectrum parts. This paper calculates the contribution corresponding to the orbital magnetic susceptibility without considering the spin splitting and effect of the spin-orbit interaction. The factors listed above are to be considered in future studies.

4. Conclusion

The spectrum of CoSi in a magnetic field near the Γ-point has been calculated. The calculation was performed in $\mathbf{k}\cdot\mathbf{p}$ approximation without and with considering the spin-orbit interaction. In the former case, the Landau levels correspond to the quasiparticles with pseudospin 1. When the spin-orbit interaction is considered in weak magnetic field, the Landau levels of the Weyl fermions and quasiparticles with pseudospin 3/2 may be distinguished in the spectrum. The appearing differences are associated with the interaction of bands.

Comparison of the Landau levels calculated in $\mathbf{k}\cdot\mathbf{p}$ approximation and tight-binding approximation showed that they match well in the region of energies above the node, and differences at lower energies are caused by the contributions of other regions of the Brillouin zone. The spectrum has the chiral Landau levels whose number corresponds to the magnitude of topological charge.

The orbital susceptibility of quasiparticles with pseudospin 1 was calculated and was demonstrated to contain two contributions. The contribution of the valence band and conduction band states appeared to be diamagnetic, it coincided with that for the Weyl quasiparticles. The contribution of the narrow middle band appeared to be paramagnetic; it prevailed when the chemical potential was near the node energy. Possible relation was noted between the contribution of topological states to the magnetic susceptibility and the experimentally observed change of sign of the susceptibility from negative to positive at a temperature decreasing to 25 K [16].

Conflict of interest

The authors declare that they have no conflict of interest.

References

[1] M.I. Fedorov, V.K. Zaitsev. Semimetals as Materials for Thermoelectric Generators. In: CRC Handbook of Thermoelectrics / Ed. D.M. Rowe. CRC Press, Boca Raton (1995).
[2] P.V. Gel'd, F.A. Sidorenko. Siliysidy perekhodnykh metallov chetvyortogo perioda. Metallurgiya, M. (1971). 583 p. (in Russian).
[3] B. Bradlyn, J. Cano, Z. Wang, M.G. Vergniory, C. Felser, R.J. Cava, B.A. Bernevig. Sci. **353**, *6299*, aaf5037 (2016).
[4] P. Tang, Q. Zhou, S.-C. Zhang. Phys. Rev. Lett. **119**, *20*, 206402 (2017).
[5] G. Chang, S.-Y. Xu, B.J. Wieder, D.S. Sanchez, S.-M. Huang, I. Belopolski, T.-R. Chang, S. Zhang, A. Bansil, H. Lin, M.Z. Hasan. Phys. Rev. Lett. **119**, *20*, 206401 (2017).
[6] D.A. Pshenay-Severin, Y.V. Ivanov, A.A. Burkov, A.T. Burkov. J. Phys.: Condens. Matter **30**, *13*, 135501 (2018).
[7] D. Takane, Z. Wang, S. Souma, K. Nakayama, T. Nakamura, H. Oinuma, Y. Nakata, H. Iwasawa, C. Cacho, T. Kim, K. Horiba, H. Kumigashira, T. Takahashi, Y. Ando, T. Sato. Phys. Rev. Lett. **122**, *7*, 076402 (2019).
[8] Z. Rao, H. Li, T. Zhang, S. Tian, C. Li, B. Fu, C. Tang, L. Wang, Z. Li, W. Fan, J. Li, Y. Huang, Z. Liu, Y. Long, C. Fang, H. Weng, Y. Shi, H. Lei, Y. Sun, T. Qian, H. Ding. Nature **567**, *7749*, 496 (2019).
[9] D.S. Sanchez, I. Belopolski, T.A. Cochran, X. Xu, J.-X. Yin, G. Chang, W. Xie, K. Manna, V. Süß, C.-Y. Huang, N. Alidoust, D. Multer, S.S. Zhang, N. Shumiya, X. Wang, G.-Q. Wang, T.-R. Chang, C. Felser, S.-Y. Xu, S. Jia, H. Lin, M.Z. Hasan. Nature **567**, *7749*, 500 (2019).
[10] A.A. Burkov. Annu. Rev. Condens. Matter Phys. **9**, *359* (2018).
[11] D.T. Son, B.Z. Spivak. Phys. Rev. B **88**, *10*, 104412 (2013).
[12] L. Schnatmann, K. Geishendorf, M. Lammel, C. Damm, S. Novikov, A. Thomas, A. Burkov, H. Reith, K. Nielsch, G. Schierning. Adv. Electron. Mater. **6**, *2*, 1900857 (2020).
[13] D.S. Wu, Z.Y. Mi, Y.J. Li, W. Wu, P.L. Li, Y.T. Song, G.T. Liu, G. Li, J.L. Luo. Chin. Phys. Lett. **36**, *7*, 077102 (2019).
[14] X. Huang, C. Guo, C. Putzke, J. Diaz, K. Manna, C. Shekhar, C. Felser, P.J.W. Moll. Appl. Phys. Lett. **119**, *22*, 224101 (2021).

[15] X. Xu, X. Wang, T.A. Cochran, D.S. Sanchez, G. Chang, I. Belopolski, G. Wang, Y. Liu, H.-J. Tien, X. Gui, W. Xie, M.Z. Hasan, T.-R. Chang, S. Jia. Phys. Rev. B **100**, *4*, 045104 (2019).
[16] S.M. Stishov, A.E. Petrova, V.A. Sidorov, D. Menzel. Phys. Rev. B **86**, *6*, 064433 (2012).
[17] V.N. Narozhnyi, V.N. Krasnorussky. JETP **116**, *5*, 780 (2013).
[18] D. Shinoda. Phys. Status Solidi A **11**, *1*, 129 (1972).
[19] S.M. Stishov, A.E. Petrova. Phys. — Usp. **54**, *11*, 1117 (2011).
[20] Y. Ishikawa, K. Tajima, D. Bloch, M. Roth. Solid State Commun. **19**, *6*, 525 (1976).
[21] N. Kanazawa. Charge and Heat Transport Phenomena in Electronic and Spin Structures in B20-Type Compounds. Springer, Jpn. (2015).
[22] G.P. Mikitik, Yu.V. Sharlai. J. Low Temperature Phys. **197**, *3–4*, 272 (2019).
[23] G.P. Mikitik, I.V. Svechkarev. Sov. J. Low Temperature Phys. **15**, *3*, 165 (1989).
[24] M. Koshino, T. Ando. Phys. Rev. B **81**, *19*, 195431 (2010).
[25] M. Koshino, I.F. Hizbullah. Phys. Rev. B **93**, *4*, 045201 (2016).
[26] G.P. Mikitik, Yu.V. Sharlai. Phys. Rev. B **94**, *19*, 195123 (2016).
[27] Y. Liu, Z. Li, L. Guo, X. Chen, Y. Yuan, F. Liu, S. Prucnal, M. Helm, S. Zhou. J. Magn. Magn. Mater. **408**, *73* (2016).
[28] C.-L. Zhang, C.M. Wang, Z. Yuan, X. Xu, G. Wang, C.-C. Lee, L. Pi, C. Xi, H. Lin, N. Harrison, H.-Z. Lu, J. Zhang, S. Jia. Nature Commun. **10**, *1*, 1028 (2019).
[29] A. Gupta. Phys. Lett. A **383**, *19*, 2339 (2019).
[30] M. Ezawa. Phys. Rev. B **95**, *20*, 205201 (2017).
[31] P. Giannozzi, S. Baroni, N. Bonini, M. Calandra, R. Car, C. Cavazzoni, D. Ceresoli, G.L. Chiarotti, M. Cococcioni, I. Dabo, A. Dal Corso1, S. de Gironcoli, S. Fabris, G. Fratesi, R. Gebauer, U. Gerstmann, C. Gougoussis, A. Kokalj, M. Lazzeri, L. Martin-Samos, N. Marzari, F. Mauri, R. Mazzarello, S. Paolini, A. Pasquarello, L. Paulatto, C. Sbraccia, S. Scandolo, G. Sclauzero, A.P. Seitsonen, A. Smogunov, P. Umari, R.M. Wentzcovitch. J. Phys.: Condens. Matter **21**, *39*, 395502 (2009).
[32] D.R. Hamann. Phys. Rev. B **88**, *8*, 085117 (2013).
[33] S. Nikolaev, D. Pshenay-Severin, Y. Ivanov, A. Burkov. Crystals **11**, *2*, 143 (2021).
[34] A.A. Mostofi, J.R. Yates, G. Pizzi, Y.-S. Lee, I. Souza, D. Vanderbilt, N. Marzari. Computer Phys. Commun. **185**, *8*, 2309 (2014).
[35] Q. Wu, S. Zhang, H.-F. Song, M. Troyer, A.A. Soluyanov. Computer Phys. Commun. **224**, *405* (2018).
[36] R. Peierls. Z. Physik **80**, *11*, 763 (1933).
[37] J.M. Luttinger. Phys. Rev. **102**, **4**, 1030 (1956).
[38] G.L. Bir, G.E. Pikus. Simmetriya i deformacionnye effekty v poluprovodnikakh. Nauka, M. (1972). 584 p. (in Russian).
[39] J.M. Luttinger, W. Kohn. Phys. Rev. **97**, *4*, 869 (1955).
[40] J.W. McClure. Phys. Rev. **104**, *3*, 666 (1956).
[41] A. Raoux, M. Morigi, J.-N. Fuchs, F. Piéchon, G. Montambaux. Phys. Rev. Lett. **112**, *2*, 026402 (2014).
[42] G. Vignale. Phys. Rev. Lett. **67**, *3*, 358 (1991).

Translated by E.Ilinskaya